Resonance Raman Studies of the Stoichiometric Catalytic Turnover of a Substrate−Stearoyl-Acyl Carrier Protein Δ^9 Desaturase Complex†

Karen S. Lyle,‡,§ Pierre Möenne-Loccoz,|| Jingyuan Ai,|| Joann Sanders-Loehr,|| Thomas M. Loehr,*,|| and Brian G. Fox*,‡

Department of Biochemistry, College of Agricultural and Life Sciences, University of Wisconsin, Madison, Wisconsin 53706-1544, and Department of Biochemistry and Molecular Biology, Oregon Graduate Institute of Science and Technology, Beaverton, Oregon 97006-8921

Received April 27, 2000; Revised Manuscript Received June 26, 2000

ABSTRACT: Resonance Raman spectroscopy has been used to study the effects of substrate binding (stearoyl-acyl carrier protein, 18:0-ACP) on the diferric centers of *Ricinus communis* 18:0-ACP Δ^9 desaturase. These studies show that complex formation produces changes in the frequencies of ν_s(Fe−O−Fe) and ν_{as}(Fe−O−Fe) consistent with a decrease in the Fe−O−Fe angle from ∼123° in the oxo-bridged diferric centers of the as-isolated enzyme to ∼120° in oxo-bridged diferric centers of the complex. Analysis of the shifts in ν_s(Fe−O−Fe) and ν_{as}(Fe−O−Fe) as a function of 18:0-ACP concentration also suggests that $4e^-$-reduced Δ9D containing two diferrous centers has a higher affinity for 18:0-ACP than resting Δ9D containing two diferric centers. Catalytic turnover of a stoichiometric complex of 18:0-ACP and Δ9D was used to investigate whether an O-atom from O_2 would be incorporated into a bridging position of the resultant μ-oxo-bridged diferric centers during the desaturation reaction. Upon formation of ∼70% yield of 18:1-ACP product in the presence of $^{18}O_2$, no incorporation of an ^{18}O atom into the μ-oxo bridge position was detected. The result with 18:0-ACP Δ^9 desaturase differs from that obtained during the tyrosyl radical formation reaction of the diiron enzyme ribonucleotide reductase R2 component, which proceeds with incorporation of an O-atom from O_2 into the μ-oxo bridge of the resting diferric site. The possible implications of these results for the O−O bond cleavage reaction and the nature of intermediates formed during Δ9D catalysis are discussed.

18:0-ACP Δ^9 desaturase (Δ9D)[1] catalyzes the O_2- and NAD(P)H-dependent introduction of a double bond between carbons 9 and 10 of 18:0-ACP to yield 18:1-ACP (*1*, *2*). This soluble homodimeric enzyme (M_r 84 000) contains a diiron cluster in each subunit. An EXAFS and Mössbauer study of resting Δ9D revealed a distribution of spectroscopically distinguishable diiron centers, with the ΔE_Q values (Table 1) and Fe−Fe distances of 3.12−3.15 and 3.41−3.43 Å consistent with the presence of both oxo- and hydroxo-bridged centers (*3*).

Previous studies of Δ9D have revealed several unique aspects of reactivity relative to other diiron enzymes. MCD studies of $4e^-$ Δ9D revealed that both iron sites of the diiron center have a 5-coordinate square pyramidal geometry (*4*), which is consistent with the geometry observed in the photoreduced crystals (*5*). However, $4e^-$ Δ9D is relatively stable in the presence of O_2 and has an autoxidation rate of <0.002 min^{-1} (*6*). For comparison, the autoxidation rates of the diferrous states of the related diiron enzymes RNR R2 Y122F (*7*, *8*) and MMOH (*9*) are $\sim10^3$-fold faster (10 and 1.3 min^{-1}, respectively).

Δ9D requires an acyl-ACP as the substrate for efficient desaturation catalysis (*6*, *10*), and the increase in reactivity observed with increased acyl chain length arises from utilization of hydrophobic binding energy to enhance catalysis (k_{cat} and k_{cat}/K_M) rather than binding (K_M) (*10*). As a physical indication of how binding energy might enhance catalysis, MCD studies revealed that the addition of stoichiometric 18:0-ACP to $4e^-$ Δ9D changed one iron site of the diiron center to a 4-coordinate distorted tetrahedral geometry while the second iron site assumed a 5-coordinate distorted trigonal bipyramidal geometry (*4*). This substrate-induced rearrangement of the diiron center produced changes in the redox-active orbitals that were postulated to enhance the reactivity with O_2 (*4*, *11*). Correspondingly, the addition

† This work was supported by the National Institutes of Health (GM-18865 to J.S.-L. and T.M.L. and GM-50853 to B.G.F.).

* To whom correspondence should be addressed. Email: loehr@bmb.ogi.edu. Telephone: (503) 748-1074. Fax: (503) 748-1464. Email: bgfox@biochem.wisc.edu. Telephone: (608) 262-9708. Fax: (608) 265-2904.

‡ University of Wisconsin.

§ Trainee of the NIH Molecular Biosciences Pre-Doctoral Training Grant T32 GM-07215.

|| Oregon Graduate Institute of Science and Technology.

[1] Abbreviations: 18:0-ACP, stearoyl-ACP; 18:1-ACP, oleoyl-ACP; Δ9D, 18:0-ACP Δ^9 desaturase; EXAFS, extended X-ray absorption fine structure; FdR, maize root NADPH:ferredoxin oxidoreductase; Fd, *Anabaena* PCC 7120 vegetative ferredoxin; G6P, glucose 6-phosphate; G6PDH, glucose-6-phosphate dehydrogenase; GC, gas chromatography; MCD, magnetic circular dichroism; MMOH, methane monooxygenase hydroxylase; resting Δ9D, as-isolated form of Δ9D containing two diferric clusters; $4e^-$ Δ9D, chemically reduced form of Δ9D containing two diiron(II) centers; peroxoΔ9D, form of Δ9D containing two μ-1,2-peroxodiiron(III) centers; peroxo-cycled Δ9D, form of Δ9D obtained from decay of peroxoΔ9D containing two μ-oxodiiron(III) centers; RR, resonance Raman; RNR R2, ribonucleotide reductase R2 component; Tyr122-O•, active site radical of RNR R2.

10.1021/bi000965v CCC: $19.00
Published on Web 08/04/2000

Table 1: Resonance Raman and Mössbauer Parameters of μ-Oxo/Hydroxo Diiron(III) Enzymes

enzyme	ν_s(Fe−^{16}O−Fe) (cm^{-1})	ν_{as}(Fe−^{16}O−Fe) (cm^{-1})	Fe−O(H)−Fe angle (deg)	δ(Fe) (mm/s)	ΔE_Q (mm/s)	doublet percentage[a]	references
peroxo-cycled Δ9D	528	733	120[b]	0.57	1.91	48	this work, (*6*, *12*)
				0.52	1.41	48	
resting Δ9D	520−521	746−747	123[b], 122[c]	0.54	1.53	72	(*16*, *37*)
			145[d]	0.49	0.72	21	
				0.50	2.20	7	
met RNR R2	493	756	108[e]	0.55	1.62	50	(*13*, *38*)
resting MMOH			88, 106[f]	0.51	1.16	48	(*39*)
				0.50	0.87	48	
ferritin				0.62	1.06	100	(*40*)
rubrerythrin	514		101[g]	0.53	1.60	100	(*41*, *42*)

[a] Percentage contribution of the indicated quadrupole doublet to the total iron content. [b] Fe−O−Fe angle calculated from RR data according to reference (*30*). [c] Fe−O−Fe angle calculated from EXAFS data for an Fe−Fe distance of 3.12−3.15 Å and an Fe−O distance of 1.79 Å. [d] Fe−OH−Fe angle calculated from EXAFS data for an Fe−Fe distance of 3.41−3.43 Å and an Fe−OH distance of 1.79−1.80 Å. [e−g] X-ray crystallography (*43*−*45*).

of O_2 to the complex of 18:0-ACP and 4e$^-$ Δ9D resulted in the stoichiometric pseudo-first-order appearance of a μ-1,2-peroxo species (*6*) at a rate of 87 s^{-1} at 24 °C (*12*), ∼10^5-fold faster than the autoxidation observed in the absence of 18:0-ACP. This intermediate has a broad optical absorption at ∼700 nm and exhibits ν(O−O) of 898 cm^{-1} in the RR spectrum (*6*). Intermediates with similar optical and RR properties have been observed in RNR R2 W48F/D84E (*13*) and ferritin (*14*). However, unlike the peroxo intermediates observed in these other diiron enzymes, the Mössbauer spectrum of peroxoΔ9D revealed asymmetric sites within the peroxodiferric center (*12*). Furthermore, in contrast to the reactivity of all other enzymic peroxodiferric complexes, decay of peroxoΔ9D was slow (0.027 min^{-1} at 25 °C), and resulted in stoichiometric formation of an asymmetric, diamagnetic diferric state termed peroxo-cycled Δ9D (*12*) without formation of 18:1-ACP and without release of H_2O_2 (*6*).

In combination, these studies suggest that the complex of 4e$^-$ Δ9D and 2 mol of 18:0-ACP assumes an arrested configuration that is capable of forming a peroxo complex but that is incapable of proceeding further into the normal desaturation cycle. However, when treated with the biological reduction system of NADPH, Fd, and FdR, the same preparations of resting Δ9D, peroxoΔ9D, or peroxo-cycled Δ9D give steady-state turnover of 18:0-ACP to 18:1-ACP with k_{cat} of 0.3−0.5 s^{-1} (*6*, *12*). To reconcile the disparate reactivities observed for chemically reduced 4e$^-$ Δ9D and biologically reduced Δ9D, we have hypothesized that the ordering of redox state changes, substrate binding, and product release have important influences on the outcome of the Δ9D reaction (*6*). In this regard, MCD (*4*) and Mössbauer photolysis (*12*) studies have shown that 18:0-ACP binding perturbs the diferrous centers, reemphasizing the potential contributions of 18:0-ACP binding to the O_2 activation step(s) required for catalysis.

Spectroscopic studies of diiron enzymes using isotopically labeled O_2 have also given insight into the coordination geometry of the diferric and peroxodiferric states (*6*, *13*−*16*), the potential rearrangements of O-atoms upon formation of reactive intermediates (*17*−*20*), as well as the fate of O-atoms upon conversion of reactive intermediates back to the resting state (*15*, *16*). Our initial RR experiments with 4e$^-$ Δ9D revealed that an O-atom derived from O_2 was not incorporated into a bridging position in resting Δ9D (*16*). However, due to uncertainties introduced by a subsequently characterized autoxidation in the absence of acyl-ACP (*6*), the question of the disposition of O-atoms from O_2 during a catalytic desaturation reaction has remained unresolved.

Here we report RR studies on the effects of 18:0-ACP binding on peroxo-cycled Δ9D and resting Δ9D. The observed shifts in vibrational frequencies indicate (1) conformational changes affecting diferric center geometry and (2) redox-associated changes in 18:0-ACP binding affinity. Furthermore, high-yield single-turnover desaturation of 18:0-ACP to 18:1-ACP does not correspond with the incorporation of an O-atom from O_2 into a bridging position of the resultant μ-oxo-bridged diferric center. These catalytic and spectroscopic results are distinct from those provided by RR and ^{17}O-ENDOR studies on the related diiron enzyme RNR R2 (*15*, *17*−*19*), suggesting an alternative route for the O−O bond cleavage step during Δ9D catalysis.

MATERIALS AND METHODS

Proteins and Reagents. Δ9D was overexpressed in *Escherichia coli* BL21 (DE3) and purified as previously described (*21*). The protein concentration was determined by optical spectroscopy (ϵ_{340} = 8400 M^{-1} cm^{-1} per dimer). Spinach apo-ACP isoform I was overexpressed in *E. coli* BL21(DE3), converted to holo-ACP by in vitro reaction with holo-ACP synthase, and converted to 18:0-ACP by reaction with *E. coli* acyl-ACP synthase (*22*). Acyl-ACP and holo-ACP were quantitated by use of 5,5′-dithiobis(2-nitrobenzoic acid) (*23*). FdR (*24*) and Fd (*25*) were overexpressed in *E. coli*, purified by standard chromatographic methods, and quantitated by optical spectroscopy (FdR, ϵ_{456} = 10 700 M^{-1} cm^{-1}; Fd, ϵ_{278} = 15 700 M^{-1} cm^{-1}). NADPH was from Sigma (St. Louis, MO) and quantitated by optical spectroscopy (ϵ_{340} = 6200 M^{-1} cm^{-1}). 18:0, G6P, and G6PDH were from Sigma. Isotopically labeled $^{18}O_2$ (97% ^{18}O content) and $^{18}OH_2$ (97% ^{18}O content) were from ICON (Summit, NJ).

Sample Preparations. Chemically reduced 4e$^-$ Δ9D (2−3 mM diiron centers) was produced as previously described (*6*, *12*). To form peroxoΔ9D, O_2 was flushed into the headspace of a Teflon septum-sealed conical-bottom reaction vial containing 4e$^-$ Δ9D. After a short equilibration time, 18:0-ACP (2−3 mM) was added and peroxoΔ9D formed rapidly. To form peroxo-cycled Δ9D, peroxoΔ9D was

exposed to air for ~2 h at room temperature, transferred to a RR capillary tube, and frozen in liquid nitrogen. To form [μ-^{18}O]peroxo-cycled Δ9D, the sample was prepared as above in $^{18}OH_2$ buffer.

To determine the exchange rate of the μ-oxo bridge, samples of resting [μ-^{18}O]-Δ9D were prepared by dilution of resting Δ9D into $^{18}OH_2$ buffer and reconcentrated using a Microcon YM30 concentrator (Millipore, Danvers, MA). Samples of resting [μ-^{18}O]-Δ9D complexed with 18:0-ACP were prepared in microfuge tubes by the addition of concentrated 18:0-ACP. The [μ-^{18}O]-enriched samples were then diluted into $^{16}OH_2$ buffer, incubated at 25 °C, transferred into a RR capillary tube at the appropriate time during the exchange reaction, and frozen in liquid nitrogen. Samples were analyzed by RR for the appearance of ν_s(Fe-^{16}O−Fe) at ~520 cm^{-1}.

Catalytic Reactions. Reactions of stoichiometric mixtures of Δ9D and 18:0-ACP were carried out in conical-bottom reaction vials at room temperature. For reaction with $^{16}O_2$, Δ9D (180 nmol of diiron centers), 18:0-ACP (180 nmol), Fd (~1 nmol), FdR (~1 nmol), and an NADPH regeneration system consisting of G6PDH (70 nmol) and excess G6P were combined in 60 μL of 100 mM phosphate, pH 7.5, containing 50 mM NaCl. The reaction vial was left open to air, and an aliquot of NADPH (10 nmol) was mixed into the solution to initiate the reaction. For RR characterization, a portion of the reaction mixture (15 μL) was transferred to a capillary tube and frozen by immersion in liquid nitrogen within 1.5 min. For 18:1 determination, a portion of the reaction mixture (5 μL) was quenched into 100 μL of tetrahydrofuran at the same time.

For reaction with $^{18}O_2$, the enzyme mixture described above was placed in a Teflon septum-sealed conical-bottom reaction vial and made anaerobic by repeated flushing and refilling with O_2-free, hydrated Ar gas. A gastight syringe was then used to introduce $^{18}O_2$ gas (~4 mL at 1 atm) into the reaction vial. The reaction was initiated by the addition of NADPH (10 nmol), and samples for RR characterization and 18:1 determination were prepared as described above within 2.5 min.

Product Determinations. The 18:0 and 18:1 thioester bonds in the tetrahydrofuran-quenched reaction mixtures were reductively cleaved to yield 18:0 and 18:1 *n*-alcohols by the addition of sodium borohydride (*26*). The fatty *n*-alcohols were extracted with chloroform and derivatized with *N*-methyl-*N*-trimethylsilyl trifluoroacetamide. The silyl ether products were analyzed (*10*) using a Hewlett-Packard 6890 GC equipped with a Hewlett-Packard 7683 auto injector and 5MS column (30 m × 0.25 mm, 0.25 μm film thickness) connected to either a flame ionization detector or a Hewlett-Packard 5973 mass sensitive detector. Under the conditions utilized, the 18:1- and 18:0-silyl ethers eluted at 15.9 and 16.5 min, respectively. The fractional desaturation was calculated by dividing the 18:1 peak area by the sum of the 18:0 plus 18:1 peak areas, and the total nanomoles of 18:1-ACP formed during the reaction was calculated by multiplying the total nanomoles of 18:0-ACP introduced into the reaction by the fractional conversion.

To ascertain the presence of $^{18}O_2$ in the appropriate reaction vials, purified toluene 4-monooxygenase (*27*) and toluene were added by a gastight syringe to the sealed reaction vial and allowed to react. The product of this reaction, *p*-cresol (*27*), was analyzed by tandem GC and electron impact ionization (70 eV) mass spectrometry for the percentage of products having either ^{16}O incorporation (m/z = 107, 108) or ^{18}O incorporation (m/z = 109, 110). Authentic standards of [^{16}O]-*p*-cresol gave two mass peaks with m/z = 107 and 108 in a nearly equal intensity ratio. To determine the fraction of $^{18}OH_2$ in isotopically enriched buffer, aniline was converted to the azido salt by treatment with HONO (*28*) and quenched with ^{18}O-containing water from the appropriate reaction mixture to yield phenol with the incorporated O-atom derived from water. This product was analyzed for isotopic content as described above.

Spectroscopic Measurements. Optical absorption spectra were obtained using a Hewlett-Packard 8452A diode array spectrophotometer. RR spectra were obtained using a custom McPherson 2061 spectrograph set to a focal length of 0.67 m, a 2 cm^{-1} spectral resolution, and a 2400 groove/mm grating. The Rayleigh scattering was attenuated by a Kaiser Optical holographic super-notch filter, and the Raman-scattered light was focused onto a Princeton Instruments liquid N_2-cooled (LN-1100PB) CCD detector. A Coherent Innova 90-6 Ar ion laser provided excitation at 350.7 nm. Spectra were obtained in a 150°-backscattering geometry from samples cooled to 15 K on the cold head of a Displex (Air Products), or from samples cooled to 90 K in capillaries inserted into a copper coldfinger in a Dewar flask filled with liquid N_2 (*29*). Absolute frequencies were obtained by calibration with powdered aspirin and CCl_4 and are accurate to ±1 cm^{-1}. Isotope shifts, obtained from spectra recorded under identical experimental conditions, were evaluated by abscissa expansion and curve resolution of overlapping bands and are accurate to 0.5 cm^{-1}.

RESULTS AND DISCUSSION

Peroxo-Cycled Δ9D Complex. Previous optical and Mössbauer titrations showed that peroxoΔ9D formation was maximized upon the addition of 1 mol of 18:0-ACP per diiron center present in 4e$^-$ Δ9D (*6*, *12*), implying tight, stoichiometric binding of 18:0-ACP. Furthermore, Mössbauer analysis revealed that decay of peroxoΔ9D to peroxo-cycled Δ9D produced asymmetric diferric centers that maintained the bound 18:0-ACP. Thus, the samples of peroxo-cycled Δ9D used to obtain the RR spectra shown in Figure 1 were produced with a similar 1:1 stoichiometry of 18:0-ACP and diiron centers. Table 1 contains a summary of the RR parameters determined from this work along with comparative spectroscopic data from other studies.

Figure 1A shows the RR spectrum obtained from 350.7 nm excitation of resting Δ9D (*16*). The features at 521 and 746 cm^{-1} correspond to ν_s(Fe−O−Fe) and ν_{as}(Fe−O−Fe), respectively. Upon the basis of earlier model studies (*30*, *31*), these features allowed us to calculate the Fe−O−Fe angle in resting Δ9D to be ~123°, a value entirely consistent with the 122° calculated from the distances for Fe−O and Fe−Fe (1.78−1.80 and 3.12−3.15 Å, respectively, for the oxo-bridged species, 72% of total iron) subsequently determined by EXAFS (*3*). Figure 1B shows the RR spectrum of resting Δ9D obtained in $^{18}OH_2$ buffer. In this spectrum, ν_s(Fe−O−Fe) and ν_{as}(Fe−O−Fe) have shifted to 504 and 712 cm^{-1}, respectively, confirming the presence of ^{18}O in the Fe−O−Fe moiety.

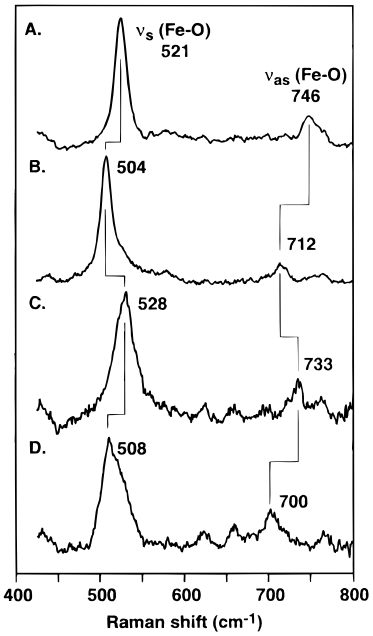

FIGURE 1: RR spectra of resting Δ9D and peroxo-cycled Δ9D. All samples were prepared in 100 mM phosphate, pH 7.5, containing 50 mM NaCl. Each spectrum was obtained 10 min after thawing as described under Materials and Methods. Samples of resting Δ9D (A, B) contained 3.0 mM diiron centers; samples of peroxo-cycled Δ9D (C, D) contained contained 3.0 mM diiron centers and 3.0 mM 18:0-ACP. The samples for (A, C) were prepared in $^{16}OH_2$ buffer; the samples for (B, D) were prepared in $^{18}OH_2$ buffer.

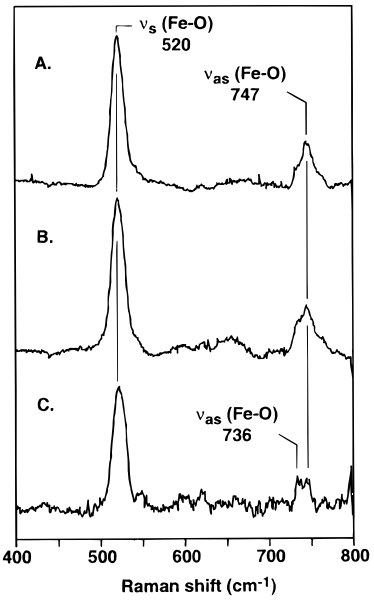

FIGURE 2: Changes in the RR spectra of resting Δ9D in the presence of various molar amounts of 18:0-ACP. (A) 0.5 mol of 18:0-ACP/mol of diferric center. (B) 1.0 mol of 18:0-ACP/mol of diferric center. (C) 3.0 mol of 18:0-ACP/mol of diferric center. A comparable spectrum obtained from a sample of resting Δ9D containing no 18:0-ACP is shown in Figure 1A. Each spectrum was obtained 10 min after thawing. Samples A and B contained 3 mM diiron centers, and sample C contained 2.6 mM diiron centers. All samples were prepared in 100 mM phosphate, pH 7.5, containing 50 mM NaCl.

Figure 1C shows the RR spectrum of peroxo-cycled Δ9D. In this spectrum, vibrational bands were observed at 528 and 733 cm^{-1}, which are also in the expected frequency range for ν_s(Fe−O−Fe) and ν_{as}(Fe−O−Fe) of a μ-oxo-bridged diferric center, respectively. When peroxo-cycled Δ9D was prepared with $^{16}O_2$ in $^{18}OH_2$ buffer, these vibrational bands shifted to 508 and 700 cm^{-1}, respectively, again confirming the presence of ^{18}O in the Fe−O−Fe moiety. The isotopic content of the buffer used to prepare the sample of Figure 3D was >80% ^{18}O as determined by reaction with the diazonium salt of aniline and subsequent mass spectral analysis of the phenol product, suggesting that only a small fraction of peroxo-cycled Δ9D would contain a μ-[^{16}O] bridge. These values of ν_s(Fe−O−Fe) and ν_{as}(Fe−O−Fe) in peroxo-cycled Δ9D are predicted to correspond to an Fe−O−Fe angle of ∼120° (*30*, *31*) and thus to a smaller Fe−Fe distance than in resting Δ9D. Therefore, the presence of 18:0-ACP in peroxo-cycled Δ9D appears to have perturbed the geometry of the diferric centers. This assessment is consistent with the Mössbauer spectra of resting Δ9D and peroxo-cycled Δ9D (Table 1), where multiple diiron species were detected in resting Δ9D, but only a single diiron species was observed in peroxo-cycled Δ9D formed in the presence of stoichiometric 18:0-ACP.

Complex of Resting Δ9D and 18:0-ACP. The role of the redox state of the diiron cluster in the formation of these complexes was also investigated in this work. In our previous studies (*6*, *12*), we have considered a half-of-the-sites model for Δ9D, where alternating subunits might be used for catalysis. As an underlying postulate of this model, a subunit of Δ9D containing a diferrous center may have higher affinity for 18:0-ACP than an ostensibly identical subunit containing a diferric center. Figure 2 shows our initial RR investigation on the effect of varying the stoichiometry of 18:0-ACP relative to the diferric centers in resting Δ9D. No redox transformations were involved in preparing the samples for the data shown in Figure 2. In Figure 2A,B, 0.5 and 1.0 mol of 18:0-ACP was added per diiron center. In these two spectra, the ν_{as}(Fe−O−Fe) band appeared only slightly broadened relative to that observed from resting Δ9D alone (Figure 1A), suggesting that only a small amount of an 18:0-ACP complex (if any) was formed at these two substrate concentrations. Figure 2C shows the RR spectrum obtained when 3 mol of 18:0-ACP was added per diiron center. In this spectrum, the ν_{as}(Fe−O−Fe) band appears to be splitting into components at 747 and 736 cm^{-1}. The ν_s(Fe−O−Fe) at 520 cm^{-1} in Figure 2C was slightly broadened toward the high frequency side, likely associated with the spectral change in the ν_{as}(Fe−O−Fe) region.

In all spectra of Figure 2, the changes observed were modest relative to those shown in Figure 1, where complete spectral conversion was obtained with a 1:1 stoichiometry of 18:0-ACP and diiron centers. Examination of a more complete saturation of 18:0-ACP binding was not undertaken in the experiments of Figure 2 because the preparation of samples suitable for spectroscopic analysis would have required impractically high concentrations of 18:0-ACP (e.g., >24 mM 18:0-ACP for a 4-fold excess). Nevertheless, comparison of the stoichiometric complex formation of Figure 1C with the partial complex formation of Figure 2C indicates that 4e$^-$ Δ9D produced to initiate formation of peroxoΔ9D must have a substantially higher affinity for 18:0-ACP than resting Δ9D.

Disposition of O-Atoms from O_2 after Single-Turnover Desaturation. Our initial study of the reaction of 4e$^-$ Δ9D

Table 2: O_2 Source, Reaction Quench Times, and Yield from Catalytic Turnover of Stoichiometric 18:0-ACP and Δ9D

reaction components[a]	O_2 source	quench time[b] (min)	% 18:1-ACP formed
Δ9D, 18:0-ACP, reductant	air	1.5	95
same as above	$^{18}O_2$	2.5	70

[a] Composition of the enzyme reaction mixture described under Materials and Methods. [b] Incubation time before freeze quench of the RR capillary or chemical quench in tetrahydrofuran. Resting Δ9D, resting Δ9D plus 18:0-ACP, and peroxo-cycled Δ9D have $t_{1/2} \approx 7$ min for exchange of the μ-oxo bridge.

in the presence of apo- and holo-ACP showed that an O-atom from O_2 did not form the oxo bridge. Subsequently, we found that purified, recombinant preparations of either apo- or holo-ACP only permitted a slow autoxidation reaction that most likely does not proceed by the same chemical mechanism as the desaturation reaction (*6*). Therefore, we have reinvestigated the fate of O-atoms from O_2 during single-turnover catalytic desaturation using 18:0-ACP, the preferred natural substrate for Δ9D.

To determine the oxo-bridge exchange rate, preparations of resting [μ-^{18}O]-Δ9D alone, resting [μ-^{18}O]-Δ9D in the presence of equimolar 18:0-ACP relative to diiron centers, and [μ-^{18}O]peroxo-cycled Δ9D were diluted into $^{16}OH_2$ buffer, and the rate of conversion from ν_s(Fe−^{18}O−Fe) to ν_s(Fe−^{16}O−Fe) was monitored. For each of these Δ9D preparations, the observed $t_{1/2}$ for the exchange reaction was ∼7 min. On the basis of this $t_{1/2}$ value, a reaction mixture that would permit complete desaturation of 18:0-ACP on a rapid time-scale (∼0.2−0.4 half time) as compared to the oxo bridge exchange reaction was assembled. By using the enzymatically driven single turnover of 18:0-ACP, less than 20% exchange of the μ-oxo bridging site would be expected at the time when the RR sample was frozen (1.5−2.5 min), making detection of the incorporation of an ^{18}O-atom from $^{18}O_2$ into a μ-oxo bridging position feasible.

As shown in Table 2, the enzymatic single-turnover desaturation of 18:0-ACP in the presence of equimolar diiron centers gave 95% conversion to product 18:1-ACP. Figure 3A shows that the ν_s(Fe−O−Fe) of 520 cm^{-1} obtained from performing this reaction in air was unlike that observed from the 18:0-ACP complex of peroxo-cycled Δ9D (528 cm^{-1}, Figure 1C). In contrast, the ν_s(Fe−O−Fe) obtained from the single-turnover desaturation reaction matched that observed from resting Δ9D in the absence of 18:0-ACP (521 cm^{-1}, Figure 1A).[2] Thus, 18:1-ACP must not have been bound in the RR sample after turnover, or if 18:1-ACP remained bound, it no longer caused a perturbation of the diiron center as monitored by the RR spectrum.

When the single-turnover desaturation was carried out under $^{18}O_2$, ν_s(Fe−O−Fe) was again observed at 520 cm^{-1}, as in resting Δ9D in the absence of 18:0-ACP (521 cm^{-1}, Figure 1A). If ^{18}O were incorprated into the bridge, a ν_s(Fe−O−Fe) of ∼500 cm^{-1} would have been observed (frequency indicated by the arrow in Figure 3B). During the $^{18}O_2$-dependent single-turnover reaction, 70% conversion of

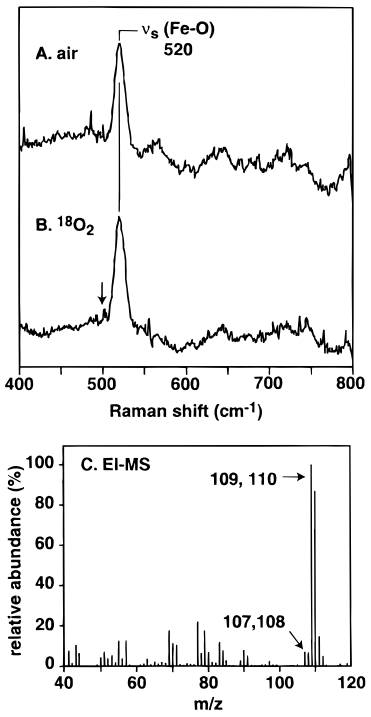

FIGURE 3: RR spectra of Δ9D after single turnover of 18:0-ACP to 18:1-ACP using either (A) ambient O_2 (air) or (B) 97%-enriched $^{18}O_2$ gas. Both samples contained 15 μM Fd, 15 μM FdR, 148 μM NADPH, and excess amounts of G6P and G6PDH in 100 mM phosphate, pH 7.5, containing 50 mM NaCl. The sample for (A) contained 3.0 mM diiron centers and 3.0 mM 18:0-ACP. The sample for (B) contained 2.6 mM diiron centers and 2.6 mM 18:0-ACP. The arrow in (B) shows the expected frequency for ν_s(Fe-^{18}O−Fe). Panel C shows a mass spectral analysis of the *p*-cresol produced when toluene 4-monooxygenase and toluene were added to the septum-sealed $^{18}O_2$-containing reaction vial after completion of the desaturation reaction. The peaks with $m/z = 109$ and 110 correspond to incorporation of an ^{18}O-atom into *p*-cresol, while the mass peaks with $m/z = 107$ and 108 correspond to incorporation of a ^{16}O-atom into *p*-cresol.

18:0-ACP to 18:1-ACP was obtained (Table 2), confirming that catalytic desaturation had taken place. Furthermore, addition of toluene 4-monooxygenase to the sealed reaction vial yielded ∼94% incorporation of ^{18}O into *p*-cresol, an O_2-dependent hydroxylation product (Figure 3C), confirming the near-exclusive availability of $^{18}O_2$ for the desaturation reaction.

Mechanistic Implications. The results shown in Figure 3 suggest that both O-atoms from O_2 were lost to solvent during a single catalytic turnover where 18:0-ACP was converted to 18:1-ACP. This result is distinct from that observed for RNR R2, where RR studies (*15*) showed the retention of ^{18}O from $^{18}O_2$ in the μ-oxo position of the diferric cluster after completion of the Tyr122-O• formation reaction and where ENDOR (*17*−*19*) studies showed the incorporation of two structurally distinct ^{17}O-atoms from $^{17}O_2$ into intermediate *X* (μ-oxo and terminal hydroxo/water positions, Figure 4A). In these previous studies of RNR R2, which encompass a resting diferric state and a reactive intermediate, the exchange of the μ-oxo bridge position was slow ($t_{1/2} >$ 5 min), whereas the ^{17}O-ENDOR study showed that the terminal hydroxo/water position exchanged within the lifetime of intermediate *X*. Since both Δ9D and RNR R2 have similar rates of exchange for the μ-oxo bridge in the diferric state, we conclude that the source of the μ-oxo bridge found

[2] In these experiments, a protein concentration sufficient for observation of ν_{as}(Fe−O−Fe) was not utilized, but this constraint does not compromise the conclusions obtained by evaluation of ν_s(Fe−O−Fe) alone.

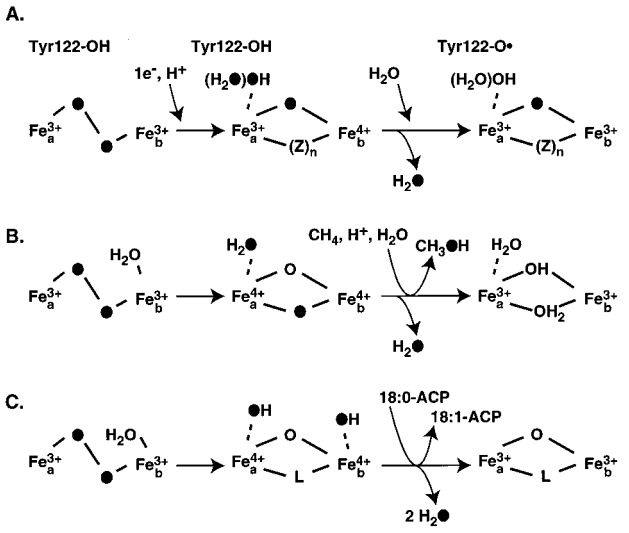

FIGURE 4: Comparison of proposed mechanisms for formation of reactive intermediates in diiron enzymes accounting for the origin of μ-oxo or hydroxo bridges. (A) The structure of peroxodiferric RNR R2 is from (*13*); the proposed structure of RNR R2 intermediate *X* and the identity of *Z* and *n* (O^{2-} or carboxylate, dependent on the protonation state of Tyr122-O• and the presence of iron-bound water or hydroxide) are from (*19*); the structure of diferric RNR R2 is from (*15*). (B) The proposed structure of MMOH compounds P and Q is from (*35, 46*); the structure of diferric MMOH is from (*43, 44*). (C) The proposed structure of peroxoΔ9D is from (*6, 12*); the proposed structure of a high-valent Δ9D species is from this work; the proposed structure of diferric Δ9D is from (*3, 6, 12, 16*). The presence of other bridging ligands indicated for Δ9D (such as a second μ-oxo or a carboxylate O-atom, designated *L*) cannot be specified.

in resting Δ9D immediately after completion of a single catalytic turnover must be an iron-bound water molecule or some other active-site water not derived from O_2.

For diiron hydroxylases, e.g., methane monooxygenase (*32*−*34*), and as shown here in control experiments for toluene 4-monooxygenase (Figure 3C), one O-atom is known to be stoichiometrically incorporated into the substrate. While the fate of the O-atom reduced to water is not known, one recent mechanism postulates heterolytic O−O bond cleavage and incorporation of one oxide-level O-atom as a μ-oxo bridge in compound Q (*11, 35*). Figure 4B summarizes this reaction sequence, which also invokes proton transfers from a metal-bound water to maintain charge neutrality and to presumably facilitate O−O heterolysis. The proton transfers would also permit migration of the metal-bound water into a μ-oxo position of the bis-μ-oxodiiron(IV) core and the migration of the heterolyzed O-atom to a terminal position, where it could be released from metal coordination as the water molecule required from the reaction stoichiometry.

Figure 4C shows one mechanism for generation of a high-valent species in Δ9D that would account for the different origin of the μ-oxo bridge during desaturation catalysis.[3] This reaction also invokes proton transfers to maintain charge neutrality within the active site, but does not lead to O-atom(s) from O_2 occupying μ-oxo bridging position(s) either in the reactive intermediates or in the diferric center produced after desaturation catalysis. We propose that this result may be achieved by the appropriate spatial combination of available coordination sites for O_2 and water on the diferrous center and by the directing influence of His and carboxylate ligands of the diiron center as the reaction cycle progresses.

In each of the three enzyme reactions shown in Figure 4, terminal hydroxo or water groups have been produced from breakage of the peroxo bond. In the RNR R2 reaction of Figure 4A, this hydroxo or water group resides on the iron(III) site of intermediate *X* (*19*), presumably closest to Tyr122-OH. In the hydroxo protonation state, this group could act as a base to assist in the formation of Tyr122-O•. In the MMOH reaction of Figure 4B, the location of the O-atom that would be transferred from compound Q to substrate during the hydroxylation step is not known. Presumably, a terminal water ligand would be rapidly exchanged and lost, while the high fidelity observed for isotopic O-atom transfer seemingly would require a regioselective approach of the substrate to one μ-oxo position of the oxidant. However, site-directed mutagenesis of toluene 4-monooxygenase, a related diiron hydroxylase (*27, 36*), has suggested that the active site residues most important for substrate orientation are found in the hydrophobic region adjacent to Fe_a (and corresponding to residues nearest to the location of Tyr122 in RNR R2), offering the alternative possibility that a terminal oxo or hydroxo group could be positioned for an O-atom transfer reaction. For the Δ9D reaction of Figure 4C, the proposed possibility for generation of terminal hydroxide moieties on both Fe_a and Fe_b of the diiron(IV) center introduces the question of whether the peroxo bond will be broken by either a homolytic or a heterolytic process. Furthermore, the identification of which iron site may react first during desaturation, if indeed the reaction proceeds in a stepwise manner, can also be investigated.

CONCLUSIONS

The focus of this work has been to use RR spectroscopy to provide information about the vibrational frequencies of the oxo-bridged diferric centers of Δ9D in the presence of 18:0-ACP. This approach has shown that 18:0-ACP binding changes the geometry of the diferric centers and that subunits containing different redox states of the diiron center may have different binding affinities for substrate. In combination, these results suggest a redox-ordered mechanism for assembly of the constituents of the catalytic complex. Furthermore, since the fate of $^{18}O_2$ consumed during a single-turnover desaturation of 18:0-ACP by Δ9D is spectroscopically distinct from that observed during Tyr122-O• formation by RNR R2 and catalytically distinct from that observed during hydrocarbon hydroxylation by the diiron hydroxylases, the intimate details of the O_2 activation steps for these three enzyme classes will likely differ, despite the substantial number of otherwise similar physical properties.

REFERENCES

1. Shanklin, J., and Cahoon, E. B. (1998) *Annu. Rev. Plant Physiol. Plant Mol. Biol. 49*, 611−641.
2. Fox, B. G. (1997) in *Comprehensive Biological Catalysis* (Sinnott, M., Ed.) pp 261−348, Academic Press, London.
3. Shu, L., Broadwater, J. A., Achim, C., Fox, B. G., Münck, E., and Que, L., Jr. (1998) *J. Biol. Inorg. Chem. 3*, 392−400.

[3] The formation of a high valent species during the desaturation reaction has not been proven; however, an intermediate of this type is reasonable considering the relative stability of the C−H bonds that must be broken to form 18:1-ACP.

4. Yang, Y.-S., Broadwater, J. A., Fox, B. G., and Solomon, E. I. (1999) *J. Am. Chem. Soc. 121*, 2770−2783.
5. Lindqvist, Y., Huang, W., Schneider, G., and Shanklin, J. (1996) *EMBO J. 15*, 4081−4092.
6. Broadwater, J. A., Ai, J., Loehr, T. M., Sanders-Loehr, J., and Fox, B. G. (1998) *Biochemistry 37*, 14664−14671.
7. Tong, W. H., Chen, S., Lloyd, S. G., Edmondson, D. E., Huynh, B.-H., and Stubbe, J. (1996) *J. Am. Chem. Soc. 118*, 2107−2108.
8. Sahlin, M., Lassmann, G., Pötsch, S., Sjöberg, B.-M., and Gräslund, A. (1995) *J. Biol. Chem. 270*, 12361−12372.
9. Lee, S.-K., Nesheim, J. C., and Lipscomb, J. D. (1993) *J. Biol. Chem. 268*, 21569−21577.
10. Haas, J. A., and Fox, B. G. (1999) *Biochemistry 38*, 12833−12840.
11. Brunold, T. C., Tamura, N., Kitajima, N., Moro-oka, Y., and Solomon, E. I. (1998) *J. Am. Chem. Soc. 120*, 5674−5690.
12. Broadwater, J. A., Achim, C., Münck, E., and Fox, B. G. (1999) *Biochemistry 38*, 12197−12204.
13. Möenne-Loccoz, P., Baldwin, J., Ley, B. A., Loehr, T. M., and Bollinger, J. M., Jr. (1998) *Biochemistry 37*, 14659−14663.
14. Möenne-Loccoz, P., Krebs, K., Herlihy, K., Edmondson, D. E., Theil, E. C., Huynh, B. H., and Loehr, T. M. (1999) *Biochemistry 38*, 5290−5295.
15. Ling, J., Sahlin, M., Sjöberg, B.-M., Loehr, T. M., and Sanders-Loehr, J. (1994) *J. Biol. Chem. 269*, 5596−5601.
16. Fox, B. G., Shanklin, J., Ai, J., Loehr, T. M., and Sanders-Loehr, J. (1994) *Biochemistry 33*, 12776−12786.
17. Burdi, D., Sturgeon, B. E., Tong, W. H., Stubbe, J., and Hoffman, B. M. (1996) *J. Am. Chem. Soc. 118*, 281−282.
18. Willems, J.-P., Lee, H.-I., Burdi, D., Doan, P. E., Stubbe, J., and Hoffman, B. M. (1997) *J. Am. Chem. Soc. 119*, 9816−9824.
19. Burdi, D., Willems, J.-P., Riggs-Gelasco, P., Antholine, W. E., Stubbe, J., and Hoffman, B. M. (1998) *J. Am. Chem. Soc. 120*, 12910−12919.
20. Valentine, A. M., Tavares, P., Pereira, A. S., Davydov, R., Krebs, C., Hoffman, B. M., Edmondson, D. E., Huynh, B. H., and Lippard, S. J. (1998) *J. Am. Chem. Soc. 120*, 2190−2191.
21. Hoffman, B. J., Broadwater, J. A., Johnson, P., Harper, J., Fox, B. G., and Kenealy, W. R. (1995) *Protein Expression Purif. 6*, 646−654.
22. Broadwater, J. A., and Fox, B. G. (1998) *Protein Expression Purif. 15*, 314−326.
23. Ellman, G. L. (1959) *Arch. Biochem. Biophys. 82*, 70−77.
24. Ritchie, S. W., Redinbaugh, M. G., Shiraishi, N., Vrba, J. M., and Campbell, W. E. (1994) *Plant Mol. Biol. 26*, 679−690.
25. Cheng, H., Westler, W. M., Xia, B., Oh, B.-H., and Markley, J. L. (1995) *Arch. Biochem. Biophys. 316*, 619−634.
26. Barron, E. J., and Mooney, L. A. (1968) *Anal. Chem. 40*, 1742−1744.
27. Pikus, J. D., Studts, J. M., McClay, K., Steffan, R. J., and Fox, B. G. (1997) *Biochemistry 36*, 9283−9289.
28. Orville, A. M., Harpel, M. R., and Lipscomb, J. D. (1990) *Methods Enzymol. 188*, 107−115.
29. Loehr, T. M., and Sanders-Loehr, J. (1993) *Methods Enzymol. 226*, 431−470.
30. Wing, R. M., and Callahan, K. P. (1969) *Inorg. Chem. 8*, 871.
31. Sanders-Loehr, J., Wheeler, W. D., Shiemke, A. K., Averill, B. A., and Loehr, T. M. (1989) *J. Am. Chem. Soc. 111*, 8084−8093.
32. Higgins, I. J., and Quayle, J. R. (1970) *Biochem. J. 118*, 201−208.
33. Froland, W. F., Andersson, K. K., Lee, S.-K., Liu, Y., and Lipscomb, J. D. (1991) in *Applications of Enzyme Biotechnology* (Kelly, J. W., and Baldwin, T. O., Eds.) pp 39−53, Plenum Press, New York.
34. Froland, W. A., Andersson, K. K., Lee, S.-K., Liu, Y., and Lipscomb, J. D. (1992) *J. Biol. Chem. 267*, 17588−17597.
35. Lee, S.-K., and Lipscomb, J. D. (1999) *Biochemistry 38*, 4423−4432.
36. Pikus, J. D., Mitchell, K. H., Studts, J. M., McClay, K., Steffan, R. J., and Fox, B. G. (2000) *Biochemistry 39*, 791−799.
37. Fox, B. G., Shanklin, J., Somerville, C., and Münck, E. (1993) *Proc. Natl. Acad. Sci. U.S.A. 90*, 2486−2490.
38. Bollinger, J. M., Jr., Krebs, C., Vicol, A., Chen, S., Ley, B. A., Edmondson, D. E., and Huynh, B. H. (1998) *J. Am. Chem. Soc. 120*, 1094−1095.
39. Fox, B. G., Hendrich, M. P., Surerus, K. K., Andersson, K. K., Froland, W. A., Lipscomb, J. D., and Münck, E. (1993) *J. Am. Chem. Soc. 115*, 3688−3701.
40. Pereira, A. S., Small, W., Krebs, C., Tavares, P., Edmondson, D. E., Theil, E. C., and Huynh, B. H. (1998) *Biochemistry 37*, 9871−9876.
41. Ravi, N., Prickrel, B. C., Kurtz, D. M., Jr., and Huynh, B. H. (1993) *Biochemistry 32*, 8487−8491.
42. Dave, B. C., Czernuszewicz, R. S., Prickril, B. C., and Kurtz, D. M., Jr. (1994) *Biochemistry 33*, 3572−3576.
43. Rosenzweig, A. C., Nordlund, P., Takahara, P. M., Frederick, C. A., and Lippard, S. J. (1995) *Chem. Biol. 2*, 409−418.
44. Elango, N., Radhakrishnan, R., Froland, W. A., Wallar, B. J., Earhart, C. A., Lipscomb, J. D., and Ohlendorf, D. H. (1997) *Protein Sci. 6*, 556−568.
45. deMaré, F., Kurtz, D. M., and Nordlund, P. (1996) *Nat. Struct. Biol. 3*, 539−546.
46. Valentine, A. M., Stahl, S. S., and Lippard, S. J. (1999) *J. Am. Chem. Soc. 121*, 3867−3887.

BI000965V